Combustion and Emissions of Gasoline, Anhydrous Ethanol and Wet-Ethanol in an Optical Engine with a Turbulent Jet Ignition System

Khalifa Bureshaid
Mechanical engineering
College of Engineering, Design and Physical Sciences
Email: Khalifa.bureshaid@brunel.ac.uk
Tel.: +447448963392

Dengquan Feng
Mechanical engineering
State Key Laboratory of Engines
Email: fengdq@tju.edu.cn
Tel.: +8615822165780

Hua Zhao
Vice Dean (Research) at Brunel University London
College of Engineering, Design and Physical Sciences
Email: Khalifa.bureshaid@brunel.ac.uk
Tel.: +4471895266698

Mike Bunce
MAHLE Powertrain, LLC
Technical Specialist - Research (RDN)
Tel.: +1 734 738-52 03

ABSTRACT

Turbulent Jet Ignition (TJI) is a pre-chamber ignition system for an otherwise standard gasoline spark ignition engine. TJI works by injecting chemical active turbulent jets to initiate combustion in a premixed fuel/air mixture. The main advantage of TJI is its ability to ignite and burn completely very lean fuel/air mixtures in the main chamber charge. This occurs with a very fast burn rate due to the widely distributed ignition sites that consume the main charge rapidly. Rapid combustion of lean mixtures leads to lower exhaust emissions due to more complete combustion at lower combustion temperature.

The purpose of the paper is to study the combustion characteristics of gasoline, ethanol and wet ethanol when operated with the pre-chamber combustion system and the ability of the pre-chamber ignition to extend the lean-burn limits of such fuels. The combustion and heat release process was analysed and exhaust emissions measured. Results show that the effect of TJI system on the lean-burn limit and exhaust emissions varied with fuels. The lean limit was extended by using fuelled pre-chamber furthest, to λ = 1.71 with gasoline, followed by λ = 1.77 with wet-ethanol and λ = 1.9 with ethanol. NOx emissions were significantly reduced with increased lambda for each fuel under stable combustion conditions. For ethanol, at maximum lean limit lambda 1.9, the NOx emissions were almost negligible due to lower combustion temperature.

Keywords: TJI turbulent jet ignition, ~~MJI Mahle jet ignition,~~ lambda air-fuel ratio, DI direct injector, PFI port fuel injector, SI spark ignition.

Formatted: Font color: Text 1

Formatted: Font color: Text 1, Not Highlight

Formatted: Font color: Text 1

1 Introduction:

There is a great deal of interest in lean burn engine technologies [1, 2, 3]. Lean burn engine operation with excess air improves the indicated thermal efficiency because of the higher specific heat ratio and reduced heat loss of lower combustion temperature. Moreover, lean burn combustion at part load operation is able to reduce the pumping losses that helps to improve the brake thermal efficiency and reduce fuel consumption. However, running an engine with a very lean fuel air mixture can be hampered by poor ignition, unstable and incomplete combustion. To overcome all these difficulties, pre-chamber has been researched and developed to operate the spark ignition engine with very fuel lean mixture by producing high temperature combustion jets from the pre-chamber to the ignite the fuel lean mixture in the main chamber [4, 5, 6, 7, 8, 9]. The pre-chamber technology was first proposed and tested by Sir Harry Ricardo in a 2-stroke engine in the beginning of the early 1900s [10], in which a pre-chamber (known and patented as turbulent head) was designed and optimised to increase the combustion process in the main chamber of a side-valve engine. Another significant early example is the torch cell engine with a pre-chamber with an auxiliary intake valve [11].

Unlike the pre-chamber design with a single throat to the main chamber , the turbulent jet ignition system works by injecting a partially quenched combusting mixture with active radicals as high turbulent jets through a number of small orifices to ignite the lean fuel mixtures in the main chamber. Jet igniters contain much smaller orifice(s) connecting the main chamber and pre-chamber combustion cavities. The smaller orifice/ orifices creates the high temperature jets that penetrate deeper into the main charge. In 1950s, the jet ignition system was proposed by Nikolai [9] and evolved by Gussak to use a small pre-chamber size [12]. Table 1 summarized the development in jet ignition system over the years.

Table. 1. Literature review of jet ignition research with small pre-chamber volumes (< 3% clearance volume).

Date	Jet Ignition System	Done by
End 1970	Jet Plume Injection and Combustion (JPIC)	Oppenheim et al. [13].
1984	Swirl Chamber Spark Plug	Reinhard Latsh [14].
1992	Hydrogen Assisted Jet Ignition (HAJI)	H.C. Watson et al. [15].
1993	Pulsed Jet Combustion	Warsaw [16].
1993	Hydrogen Flame Jet Ignition (HFJI)	Toyota College [17].

1999	Self-Ignition Triggered by Radical Injection (APIR)	University of Orleans [18].
1999	BPI- Bowl Pre-Chamber Ignition	University of Karlsruhe and Multitorch [19]
2003	Pulse Jet Igniter (PJI)	Najt et al. [20]
2005	Homogenous Combustion jet Ignition (HCJI).	Robert Bosch. [21]
2007	IAV Pre-Chamber Spark Plug with Pilot Injection.	IAV GmbH and Multitorch [22].
2009	Turbulent Jet Ignition (TJI).	Mahle Powertrain [4].

Formatted: Font color: Text 1

Formatted: Font color: Text 1, Not Highlight

Formatted: Font color: Text 1

In this research, a Mahle Jet Ignition (MJI) unit was used, which features a much smaller pre-chamber than the previous pre-chamber designs (< 5% of main chamber volume at TDC) to reduce the heat loss. Further, small pre-chamber surface emits fewer hydrocarbon (HC) emissions due to the reduced crevice volume and combustion surface area. Figure 1 and 2 display computer design images of the pre-chamber installed in the optical engine. By using small orifice diameter, it helps to quench the injected flame from pre-chamber to main chamber. Besides that, the quenching flame enters the main chamber with high turbulent that allows jets to go deeper into the main charge and to fully burn main chamber charge. Also, turbulent jet flows ensures the interaction between radicals and main chamber charge. Both chambers can be fuelled with two separate fuel systems. The main chamber was fuelled by a PFI injector and the pre-chamber by a slim DI injector. The benefit of fuelling pre-chamber with DI injector is to allow precise and de-coupled control over the mixture in both chambers. Multi-orifices gives more combustion sites in the main chamber. Further review of the MTJI pre-chamber design can be found in [23, 24, 25].

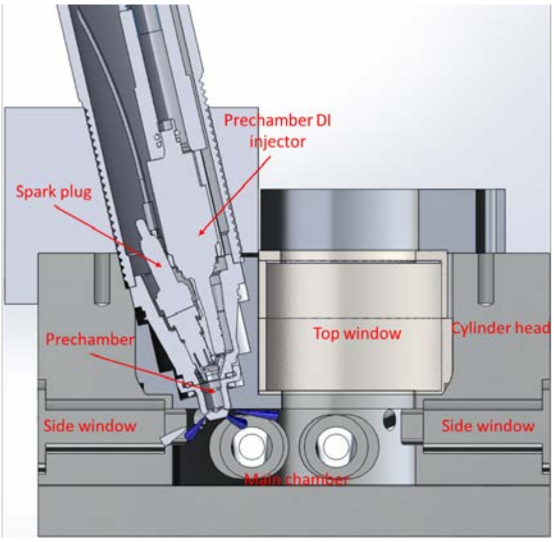

Figure 1 Sectioned view of the MJI unit installed in the optical engine

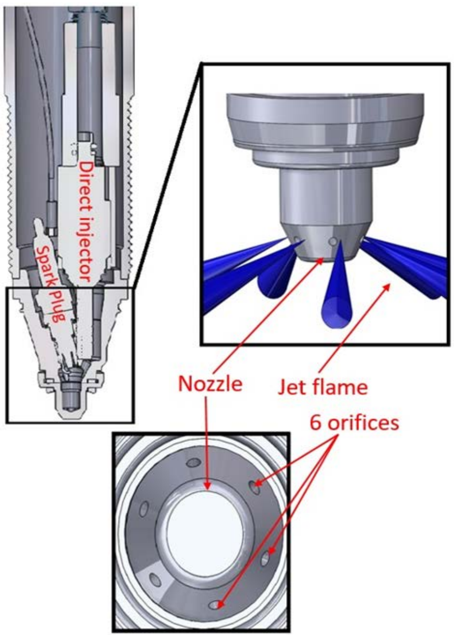

Figure 2. Design image shows the MJI pre-chamber and nozzle inside.

Previous works about the effect of jet ignition system in combustion engines mainly concentrated on engine performance and engine exhaust out emissions. There are limited publications presenting detailed optical results on the in-cylinder flame propagation mechanisms of biofuels such as ethanol and wet-ethanol by using the jet ignition system. Ethanol and wet ethanol offer a good option to suppress knocking because of their higher RON and MON. Besides, their higher latent heat of vaporization reduce the charge temperature, especially in direct-injection engines.

The purpose of the paper is to study the combustion characteristics of gasoline, ethanol and wet ethanol when operated with the pre-chamber combustion system and the ability of the pre-chamber ignition to extend the lean-burn limits of such fuels. In addition to gain further understanding of the jet formation and their effect on the combustion in the main chamber through in-cylinder high speed imaging, the current work aims to study the combustion characteristics of anhydrous ethanol and wet ethanol under different air-fuel ratios by using jet ignition system. Differences in engine performance, heat release and combustion, and flame propagation are compared and benchmarked with results of conventional gasoline, by simultaneous in-cylinder pressure measurements and high-speed flame chemiluminescence imaging.

2 Experimental Setup

During this research, a customized single cylinder optical engine was used with its cylinder head modified for the MTJ installation. The bottom-end of the engine is based on a commercial Lister Petter TS1 with a modified flat piston crown. Both intake and exhaust valves are located on the sides so that a full view of the combustion chamber can be realised by the installation of an optical window at the top. As shown in Figure 3, in order to fit the MJI unit, the cylinder head was modified by splitting the top of the cylinder head into two parts. The MTJ unit was installed in one side and a half circular window on the other side for the optical access from the top. In addition, two optical windows flush mounted at the top of the cylinder block can be used to gain the optical access from the side. The quartz windows are designed to withstand peak in-cylinder pressure up to 150 bar.

Formatted: Font color: Text 1

Formatted: Font color: Text 1, Not Highlight

Formatted: Font color: Text 1

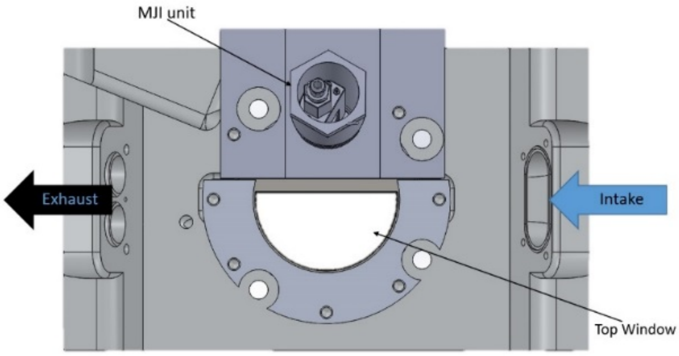

Figure 3 Schematic view of cylinder head

The basic geometry of the engine is provided in Table 2. The engine has two inlet and one exhaust valves. To maintain realistic valve durations and overlap, the side mounted poppet valves are recessed into special cylindrical pockets within the chamber side walls.

Table. 2. Basic engine geometry

Parameter	Value (unit)
Displacement	631 cc
Cylinder	1
Bore	95 mm
Stroke	89 mm
Compression Ratio	8.4:1
Exhaust valve	140/370 (°aTDC)
Valve overlap	25 (CA)
Inlet valve	345/575 (°aTDC)
Valve lift	5 mm

The ignition system in the main chamber comprises of an NGK ER9EH 8mm spark plug and a Bosch P100T ignition coil. The engine is coupled to a 10kW DC motor dynamometer via a flexible coupling. The fuel in the main chamber is supplied from a 5.0 litre fuel tank at 3 bar gauge pressure and injected into the intake port by a Bosch EV6 Port fuel injector installed in front of the intake valve. A filter was fitted between the fuel tank and the pump to remove the majority of particles from fuel. The in-cylinder pressure was measured by an AVL piezoelectric pressure transducer (GH14DK) and charge amplifier and its output was recorded and digitised by a high-speed USB type LabVIEW data-logging card (DAQ) at four samples per crank angle degree via a digital shaft encoder that connected to the intake camshaft. To determine the overall air/fuel ratio, a Bosch LSU 4.2 UEGO sensor (Universal Exhaust Gas Oxygen sensor) was fitted to the exhaust pipe. The UEGO sensor was connected to an

ETAS LA4 lambda meter. The intake plenum absolute pressure was recorded by a Gems 1200 series CVD sensor. The intake and exhaust temperatures were measured by k-type thermocouples which were fitted downstream of the inlet air heater and in the exhaust ports respectively. The heat release analysis was performed by using an in-house MATLAB program on the averaged cylinder pressure over 300 cycles, recorded in discrete 100 cycle batches. The ignition system for MJI comprises an NGK ER9EH 8mm spark plug and Bosch P100T ignition coil. Fuel injection into the pre-chamber is achieved by a small DI injector at 70 bar from a high pressure air driven diaphragm pump.

Combustion images were captured through the top window via a 45° mirror by a MEMRECAM fx6000 high speed video camera at 6000 frames per second (fps) with a resolution of 512 x 384 pixels, as shown in Figure 4. The start of camera imaging was triggered by the spark ignition signal. At constant test speed 1200 rpm, the imaging interval can be calculated to be 1.2 CAD. According to the ignition timing and the sampling interval, the images timing sequences can be known and linked to the in-cylinder pressure data. The gamma and gain of the camera were adjusted for each test to improve the clarity of the images.

Formatted: Font color: Text 1

Formatted: Font color: Text 1, Not Highlight

Formatted: Font color: Text 1

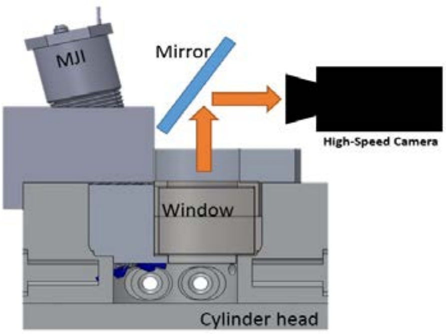

Figure.4 Schematic view of the optical engine and high speed imaging system.

Table 3 summarize the properties of the fuels tested. The differences in fuel properties affect the fuel burning and combustion process. For instance, because of their higher research octane number, anhydrous ethanol and wet ethanol are less prone to knocking combustion than gasoline. Wet-ethanol (5% water) shows the ability to resist the knocking combustion than anhydrous ethanol gasoline blends [26]. In addition, their higher latent heat of vaporization reduces the charge temperature, especially in direct-injection engines. However, the lower caloric value of ethanol in volume is only around 72% compare to gasoline. Under fixed engine speed and load condition, around 1.61 times more volumetric ethanol is required due to its relative low stoichiometric ratio. Combining above two aspects, totally 1.16 times greater volumetric energy is contained when stoichiometric ethanol/air mixture is utilized. To produce a stable combustion in the pre-chamber for the subsequent jet ignition of lean or diluted mixture in the main chamber, a slightly rich or stoichiometric mixture is prepared in the pre-chamber.

Table 3 The physical-chemical characteristics for Gasoline, ethanol and hydrous [27,28].

Property	Gasoline	Anhydrous Ethanol	Wet ethanol
Chemical formula	CnH1.87n	C_2H_5OH	10% water in ethanol (E90W10)
Density (1bar, 21ºC)	0.74 kg/liter	0.79 kg/liter	0.816 kg/litre
Lower heating value	41.087 MJ/kg	28.865 MJ/kg	25.318 MJ/kg
Latent heat of vaporization (kJ/kg).	305	840	-
Reid vapor pressure	1.03 bar	0.18 bar	-
Volumetric energy	31.6 MJ/liter	22.8 MJ/liter	21.18 MJ/liter
Stoichiometric AFR	14.421	8.953	7.853
Oxygen content	0	34.8	36.42
RON	97	109	106

Among this research, the combustion engine was connected to Horiba MEXA-584L automotive emission analyser that is able to measure CO, HC and NOx emissions. Before sampled emissions results, the Horiba MEXA-584L automotive emission analyser was calibrated so that it complies with international slandered ISO 3930/ OIML R99 (2000) class 0. The output of HC provided by the gas analyser was on a Carbon 6 (C6) basis. Where, the HC results were converted to C1.

3 EXPERIMENTAL TEST CONDITIONS

All experiments were carried out at 1200 rpm and wide-open-throttle (WOT) with gasoline, hydrous and wet ethanol. Table 4 shows the test conditions for all experiments. For each fuel, the following three combustion modes were studied; (1) conventional spark ignition combustion without the pre-chamber, (2) spark ignition in the pre-chamber without additional fuel injection in the pre-chamber, (3) spark ignition in the pre-chamber with additional fuel injection. For each combustion mode, after warming up the engine, the spark timing was adjusted to find the MBT at lambda 1. Then, the fuel amount was reduced and MBT spark timing found until the maximum lean burn limit defined by

COVIMEP ≤ 5%. The fuel injection in the pre-chamber was set at 50 °CA before the spark discharge to allow for the mixture formation taking place.

The pre-chamber injection fuel was set to 0.3, 0.5 and 0.5 mg/pulse for gasoline, ethanol and wet-ethanol respectively, to achieve stable combustion of the leanest air/fuel mixture in the main chamber as measured by the highest overall lambda. The pre-chamber air mass was calculated based on mean gas temperature. The in-cylinder temperature, pressure and composition are effectively modelled as homogeneous at each instant of time. The gas medium is assumed to obey the perfect gas law. Information has been added into the manuscript. Then the lambda values of pre-chamber mixture were estimated to be 0.78, 0.9 and 1 for gasoline, ethanol and wet-ethanol, respectively. It is note that the thermodynamic state within the pre-chamber at the time of injection was about 5 bar and 550 K. The pre-chamber volume is 1 cm^3 which is only 1.27 % of the main chamber volume at TDC.

Table 4 Test condition.

Speed	1200 rpm
Fuel	Gasoline (baseline, Ethanol and Wet-ethanol)
Spark timing	MBT/Lean-burn Limited
End of pre-chamber injection	50-70 °CA bTDC
Compression ratio	8.4
Inlet pressure	1 bar
Lambda (λ)	1 to maximum λ (until COV_{IMEP} ≥ 5).

4 Results and Discussions

4.1 Effect of fuel on IMEP and the lean-burn limit

Figure 6 shows the maximum lean-burn limit for each of the combustion modes of gasoline, ethanol and wet-ethanol. The normal SI combustion mode started with lambda 1 and spark ignition in the main chamber at the MBT spark timing. Then, the amount of fuel was decreased until the lean-burn limit was reached with spark ignition in the main chamber. It can be seen that the engine was able to operate with the highest Lambda with ethanol fuel using spark ignition in the main chamber. This is caused by the relatively faster burning rates of ethanol [28].

As shown in Figure 5, the maximum relative air/fuel ratio or Lambda was extended slightly for all three fuels when the spark ignition took place in the pre-chamber without pre-chamber fuel injection. This can be explained by the ~~pre-chamber is fed a pre-mixed air/fuel mixture~~multiple ignition sites by the

Formatted: Font color: Text 1
Formatted: Font color: Text 1, Not Highlight
Formatted: Font color: Text 1
Formatted: Font color: Text 1
Formatted: Font color: Text 1, Not Highlight
Formatted: Font color: Text 1
Formatted: Font color: Text 1, Not Highlight

high temperature turbulent jets from the ~~main chamber due to the piston motion and subsequent flow interaction between both combustion cavities~~pre-chamber after the ignition in the pre-chamber. ~~The multiple ignition and combustion sites caused by the turbulent high temperature jets of high temperature gas from the pre-chamber produce high energy products from this combustion event, then transferred to the main chamber after the combustion has started in the pre-chamber.~~

Formatted: Font color: Text 1

The most significant extension to the lean-burn limit was achieved by the addition of fuel injection in the pre-chamber. As it will be shown later by the heat release analysis and combustion images, the ignition of the near stoichiometric mixture in the pre-chamber resulted in much faster combustion of the mixture in the main chamber as a result of multiple ignition sites by the highly active gas jets emanating from the pre-chamber nozzle holes. These jets of radicals enter the main chamber with high turbulent and temperature to ignite the main chamber charge at multiple sites and subsequent multiple flames in the chamber.

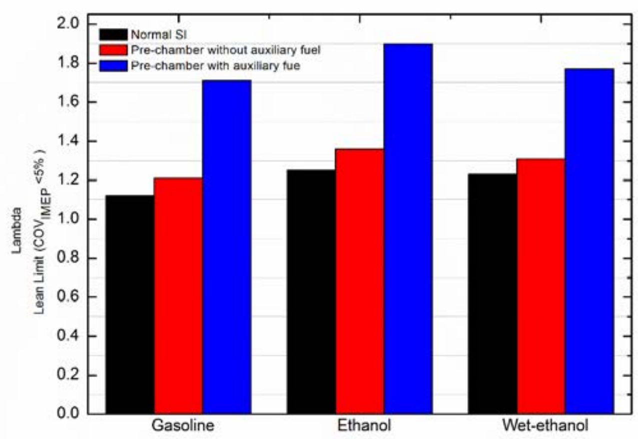

Figure 5 Comparison of lean Limit (5% CoV_{IMEP}) between normal SI spark and pre-chamber ignition (with and without auxiliary fuel) combustion systems for gasoline, ethanol and wet-ethanol

Figure 6 illustrates the variation in IMEP with different fuels and lambda at 1200 rpm and inlet pressure 1 bar with fuel injection in the pre-chamber. The IMEPnet values shown in the figure are related to maximum lambda that pre-chamber could achieve with stable combustion where the corresponding net IMEP recorded at the MBT spark timing of each fuel. The IMEP values decreased with increasing lambda as less fuel was injected. However, IMEP values of all three fuels are similar and IMEP of ethanol was slightly higher followed by wet-ethanol and gasoline. These results based on the difference in the energy input of each fuel. As mention above, in case of constant volumetric air flow rate the input energy contained in a stoichiometric mixture of one kilogram of intake air and fuel are 2.92, 3 and 3 MJ for gasoline, ethanol and wet ethanol, respectively. The gasoline engine operation was conducted and limited to lambda of 1.7. As the lambda exceeded than the lean limit 1.7, more and more cycles became misfiring and partial burn, as indicated by the high COV of IMEP of more than 5% in Figure 7. From the figure it can be seen that ethanol shows more stable combustion and extends the lean limit to λ = 1.9 followed by wet-ethanol with lambda at 1.77.

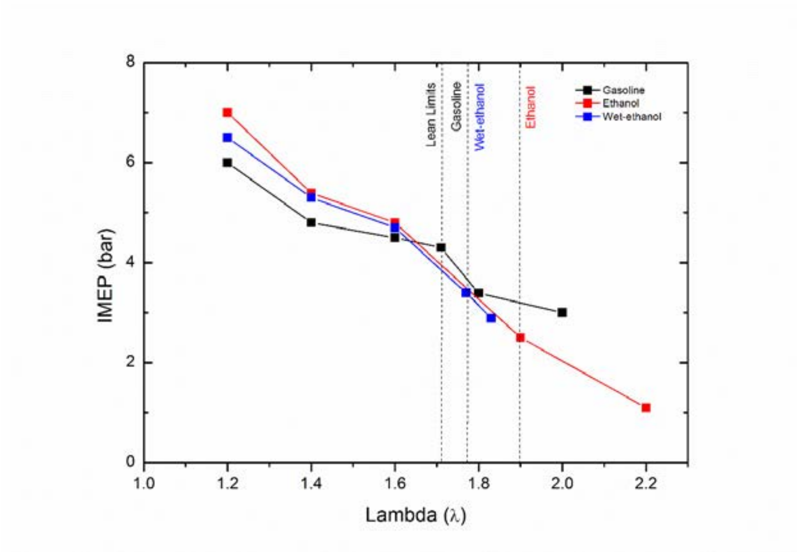

Figure 6 Effect of air/fuel ration for each fuel on IMEP variation with pre-chamber fuel injection

Formatted: Font color: Text 1, Not Highlight

Formatted: Font color: Text 1

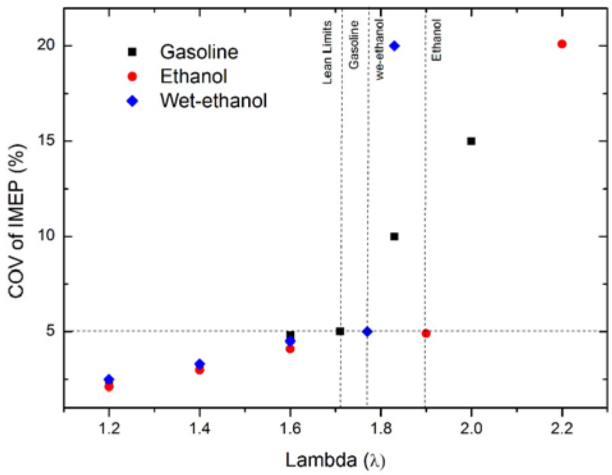

Figure 7 Effect of air/fuel ratio for each fuel on combustion stability. At 1200 rpm, inlet pressure 1 bar.

5.2 Comparison of exhaust emissions

As Figure 8 shows the NOx emission was reduced with increased lambda due to lower combustion temperature. Gasoline combustion produced the highest NO emission followed by the wet ethanol and then ethanol. This can be explained by the advanced spark timing and higher peak cylinder pressure and temperature results shown in Figure 11 and Figure 13. The latent heat of vaporization of ethanol can also contribute to their lower NOx emission. For ethanol the NOx emissions became extremely low at the lean limit lambda 1.9 as the maximum combustion temperature dropped below 1800K. Temperature here refers to the in-cylinder mean gas temperature, which was calculated based on a standard single-zone model according to the measured pressure.

Formatted: Font color: Text 1, Not Highlight

Formatted: Font color: Text 1

Formatted: Font color: Text 1, Not Highlight

Formatted: Font color: Text 1

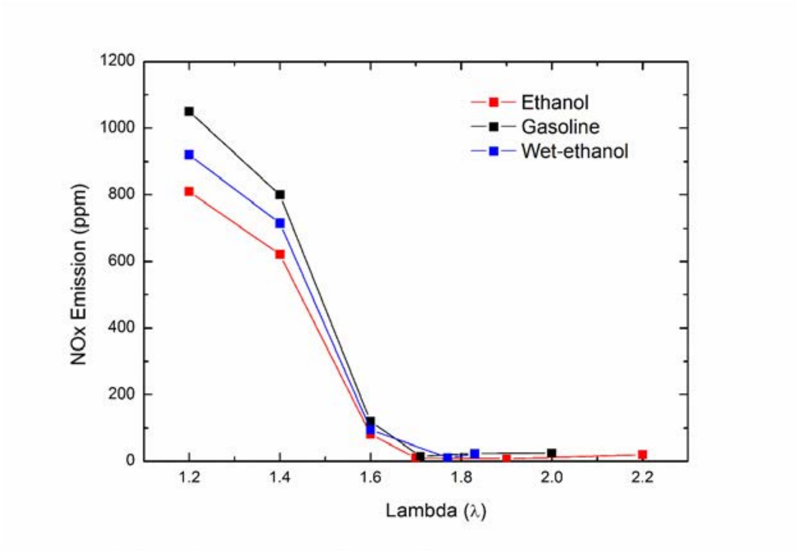

Figure 8 Effect of air/fuel ratio on NOx emissions at inlet pressures 1 bar, 1200 rpm maximum lean and MBT Spark timing with fuel pre-chamber

Formatted: Font color: Text 1, Not Highlight

Formatted: Font color: Text 1

Figure 9 shows the HC emissions result for gasoline, ethanol and wet-ethanol at MBT spark timing, inlet pressure 1 bar and 1200 rpm. Mechanisms of HC changes were thought to be correlated to the in-cylinder combustion temperature and the combustion efficiency. When lambda was increased, lean combustion resulted in lower engine load and thereby lower in-cylinder temperature, which lead to increase of HC emissions at lean condition. On the other hand, lean combustion tend to cause unstable combustion and generate more HC emissions, which can be indicated by the COV of IMEP under lean condition. Evidence of IMEP and COV can be found in Figure 6 and Figure 7, respectively. Ethanol shows the lower level of HC emissions due to its faster flame speed and shorter combustion duration shown in Figure 11 and Figure 12. Combustion was faster and that leads to reduce the HC emissions. Due to the lean combustion is running with excess air, the CO emissions are very low. The CO emission results follow the similar trend as the HC emissions for the same reasons.

Formatted: Font color: Text 1, Not Highlight

Formatted: Font color: Text 1

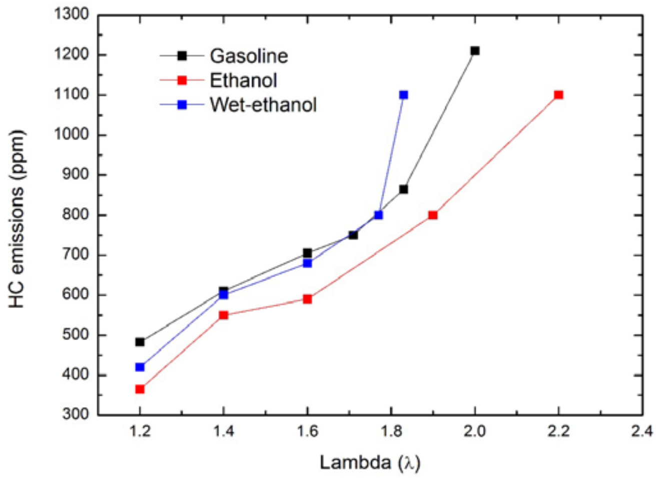

Figure 9 Effect of air/fuel ratio for each fuel on HC emissions at inlet pressures 1 bar, 1200 rpm maximum lean and MBT Spark timing with fuel pre-chamber.

Formatted: Font color: Text 1, Not Highlight

Formatted: Font color: Text 1

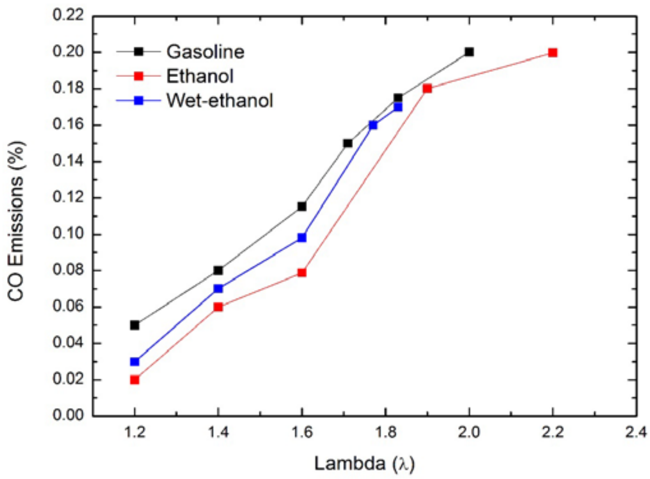

Figure 10 Effect of air/fuel ratio for each fuel on CO emissions at inlet pressures 1 bar, 1200 rpm maximum lean and MBT Spark timing with fuel pre-chamber

Formatted: Font color: Text 1, Not Highlight

Formatted: Font color: Text 1

5.3 Comparison of the Combustion and heat release processes

Figures 11 and 12 show the initial heat release process and main combustion duration expressed as the mass fraction burned (MFB) 0-10% (CA 0-10) and crank angle 10-90% (CA 10-90), respectively. It can be seen that both the initial heat release process and main combustion duration increased with leaner mixture and ethanol burned at a faster rate with retarded MBT timings. The difference in the MBT timing became greater with increased lambda.

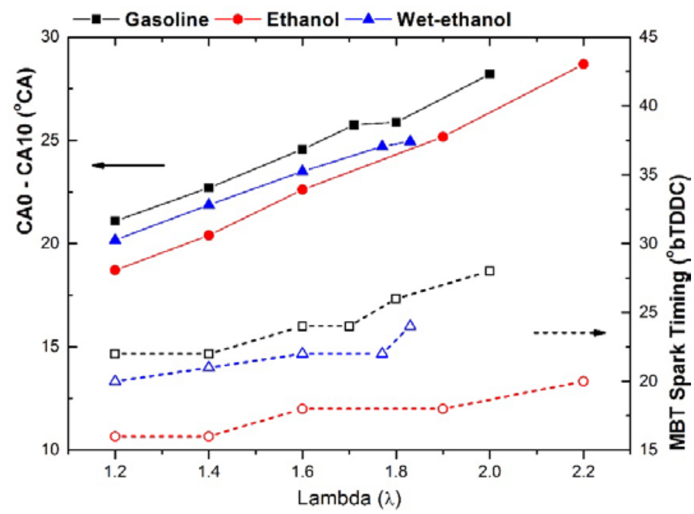

Figure 11 Effect of fuel on 0 – 10% mass fraction Burned (MFB). At inlet pressure 1 bar, 1200 rpm and MBT spark timing.

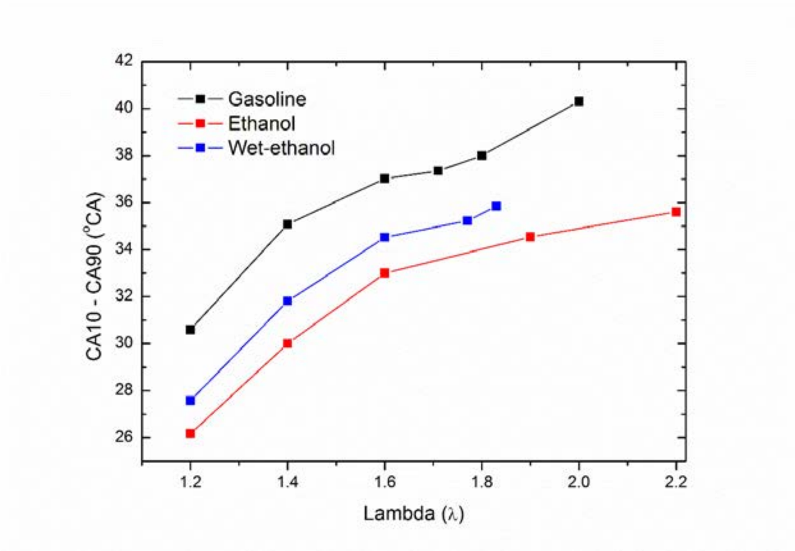

Figure 12 Effect of pre-chamber fuel on 10 –90% mass fraction Burned (MFB)

Figure 13 plotted the in-cylinder pressures traces and the corresponding heat release rates of each fuel operating at different air-fuel ratios. Without auxiliary fuel injection into pre-chamber, peak cylinder pressure of main chamber consistently declined when lambda increase from 1.2 to 1.6. When the auxiliary fuel was injected into pre-chamber to reach the maximum lean condition, cylinder pressure slightly increased despite leaner mixture was used in the main chamber. As indicated by the heat release rate curves, the start of combustion was advanced and the initial development was promoted when auxiliary fuel was provided into the pre-chamber.

Table 5 Test condition.

	Gasoline	Ethanol	Wet-ethanol
Using unfuelled pre-chamber	Lambda 1 ~1.2	Lambda 1 ~1.2	Lambda 1 ~1.2
Using unfuelled pre-chamber	Lambda 1.4 ~ lean limit (1.71)	Lambda 1.4 ~ lean limit (1.9)	Lambda 1.4 ~ lean limit (1.77)
Inlet pressure (bar)	1 bar	1 bar	1 bar
Speed (rpm)	1200	1200	1200
End of pre-chamber injection (°CA)	50	50	50
The pre-chamber injection fuel (mg/pulse)	0.3	0.5	0.5

Formatted: Font color: Text 1

Formatted: Font color: Text 1, Not Highlight

Formatted: Font color: Text 1, Not Highlight

Formatted: Font color: Text 1, Not Highlight

Formatted: Font color: Text 1, Not Highlight

Formatted: Font color: Text 1, Not Highlight

Formatted: Font color: Text 1, Not Highlight

Formatted: Font color: Text 1, Not Highlight

Formatted: Font color: Text 1

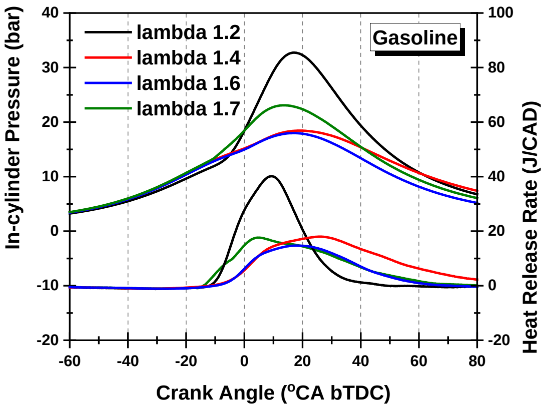

(a) Gasoline at lambda 1.2, 1.4, 1.6 and 1.7.

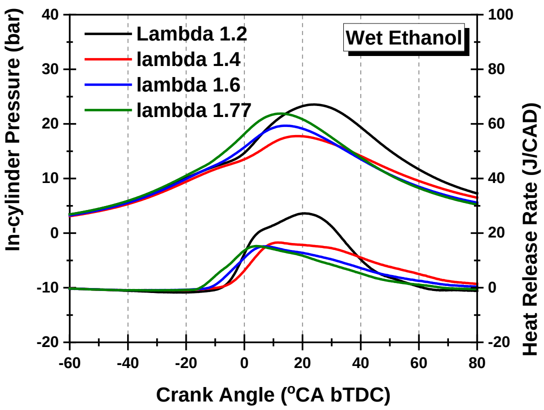

(b) Wet ethanol at lambda 1.2, 1.4, 1.6 and 1.77.

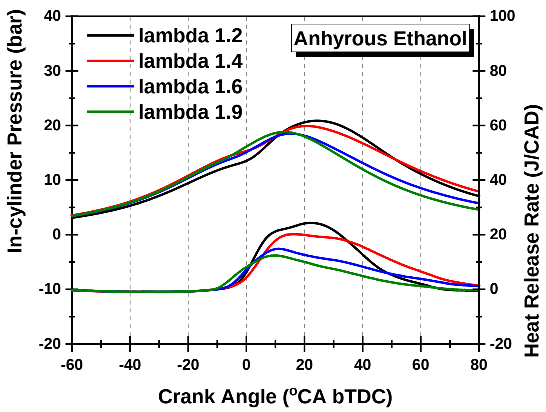

(c) Anhydrous ethanol at lambda 1.2, 1.4, 1.6 and 1.9.

Figure 13 In-cylinder pressure and heat release rate at different lambda: (a) Gasoline, (b) Wet ethanol and (c) Anhydrous ethanol.

5.4 Imaging results

As previously mentioned, a high speed video camera was used to capture the flame propagation process through the half circle window at 6000 fps, producing a temporal resolution of 1.2 °CA between adjacent frames. All the images were taken with lambda fixed at 1.3 and spark timing at 22 °CA bTDC. Figure 14 shows typical flame propagation images at different crank angles of gasoline, ethanol and wet ethanol. It was notice that the enflamed area for ethanol is bigger than wet-ethanol and gasoline at the same crank angle timing.

The flame images were then converted into binary images to calculate the flame radius, flame speed and shape factor, as shown in Figure 15. Mean flame radius and flame speed of each fuel are shown in figures 16 and 17, respectively. The flame radius is calculated based on the measured flame area of the binary flame images averaged over 30 cycles. It can be seen that ethanol flame expands at the highest speed followed by wet-ethanol and gasoline, consistent with the heat release results. For instance, at 10.8 °CA aTDC the speed of flame was measured to be 57.28, 52.20 and 35.98 m/s for ethanol, wet-ethanol and gasoline, respectively. Please note that half of the optical window has to be blocked in order to mount the pre-chamber ignition system. Therefore, the ignition near the pre-chamber tip and the initial flame development couldn't be visualized. In this case, the image sequences started at the middle of the flame propagation and the flame speed continuously decreased at the end of combustion.

Formatted: Font color: Text 1

Formatted: Font color: Text 1, Not Highlight

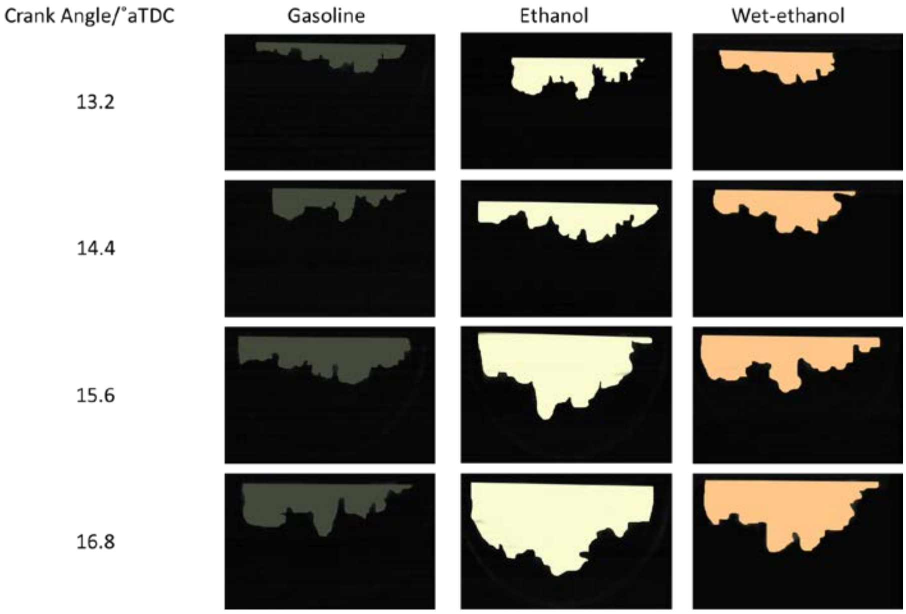

Figure 14 Images of flame propagation of different fuels at lambda 1.3 and spark timing 22 ^{o}CA bTDC.

Figure 15 the stages of image processing (from left to right the original natural light image, the selected parameter and binarised image).

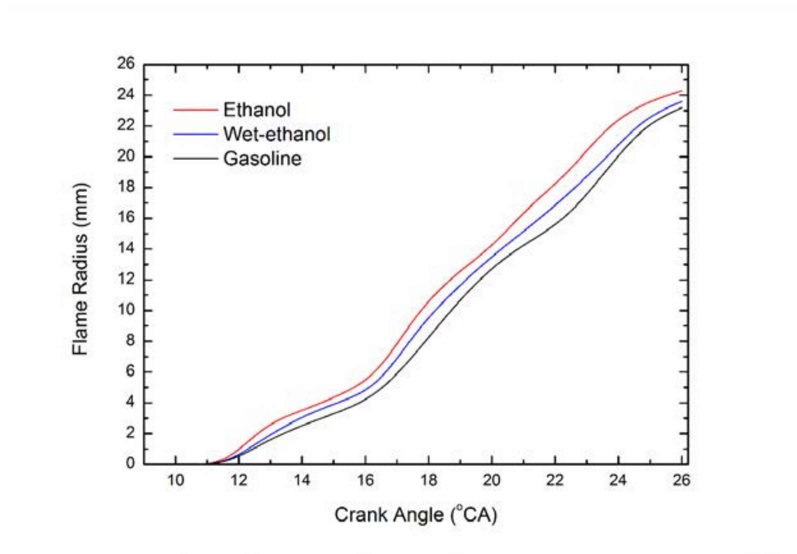

Figure 16 Effect of fuel on mean flame radius development

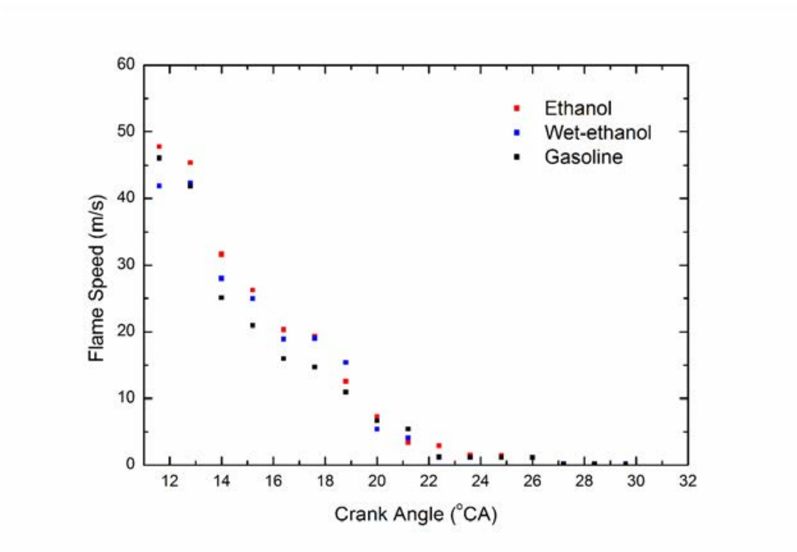

Figure 17 Effect of fuel on the flame speed.

<u>7 SUMMARY</u>

Engine experiments were carried out to study the effect of turbulent jet ignition from a small pre-chamber in a single cylinder optical engine fuelled with gasoline, anhydrous ethanol and wet ethanol. The presence of multiple high temperature turbulent gas jets significantly extended the lean-burn limits of all three fuels as well as shortening the combustion duration with retarded MBT spark timing. The most extended lean-burn operation was achieved with ethanol at a lambda of 1.9. In addition, ethanol and wet ethanol produced higher IMEP because of their faster combustion and heat release process, as shown by the initial heat release and main combustion duration, CA0 - CA10 and CA10 – CA90 results. Even with 10% water, the wet ethanol could still burn faster and produce better engine performance than gasoline.

The extended lean-burn limits by the turbulent jet ignition also led to significant reduction in NO emissions. When operated at lambda 1.9, little NOx emission was produced from the ethanol fuel. In general, both anhydrous and wet ethanol fuels produced lower NO, HC and CO emissions than gasoline as the combustion temperature was lowered and combustion become more stable and complete than those of gasoline combustion.

The high speed combustion chemiluminescence imaging provided the direct evidence of the multiple combustion sites in the main chamber as a result of the high temperature turbulent ignition jets and illustrated that ethanol had the fastest flame speed followed by wet-ethanol and gasoline.

6 Acknowledgments

Acknowledgments are due to Mahle Powertrain that supported this project. The author thank Mr. Mike Bounce (Technical Specialist - Research (RDN) at Mahle Powertrain) for his precious help and technical support.

8 References

1. Tully, E. and Heywood, J., "Lean-Burn Characteristics of a Gasoline Engine Enriched with Hydrogen Plasmatron Fuel Reformer," SAE Technical Paper 2003-01-0630, 2003, https://doi.org/10.4271/2003-01-0630.
2. Toulson, E., Watson, H., and Attard, W., "The Lean Limit and Emissions at Near-Idle for a Gasoline HAJI System with Alternative Pre-Chamber Fuels," SAE Technical Paper 2007-24-0120, 2007, https://doi.org/10.4271/2007-24-0120.
3. Cairns, A., Stansfield, P., Fraser, N., Blaxill, H. et al., "A Study of Gasoline-Alcohol Blended Fuels in an Advanced Turbocharged DISI Engine," SAE Int. J. Fuels Lubr. 2(1):41-57, 2009, https://doi.org/10.4271/2009-01-0138.

4. Dale, J. D., Checkel, M. D. and Smy, P. R., "Application of High Energy Ignition Systems to Engines", Progress in Energy and Combustion Science, 1997. 23 (5-6), 379-398.
5. Chinnathambi, P., Bunce, M., and Cruff, L., "RANS Based Multidimensional Modeling of an Ultra-Lean Burn Pre-Chamber Combustion System with Auxiliary Liquid Gasoline Injection," SAE Technical Paper 2015-01-0386, 2015, doi:10.4271/2015-01-0386.
6. Attard, W. and Blaxill, H., "A Lean Burn Gasoline Fueled Pre-Chamber Jet Ignition Combustion System Achieving High Efficiency and Low NOx at Part Load," SAE Technical Paper 2012-01-1146, 2012, https://doi.org/10.4271/2012-01-1146.
7. Bunce, M. and Blaxill, H., "Methodology for Combustion Analysis of a Spark Ignition Engine Incorporating aPre-Chamber Combustor," SAE Technical Paper 2014-01-2603, 2014, doi:10.4271/2014-01-2603.
8. Heywood, J.B., Automotive Engines and Fuels: A Review of Future Options. Progress in Energy and Combustion Science, Vol. 7, Iss. 3., pp.155-184, 1981.
9. Bunce, M., Blaxill, H., Kulatilaka, W., and Jiang, N., "The Effects of Turbulent Jet Characteristics on Engine Performance Using a Pre-Chamber Combustor," SAE Technical Paper 2014-01-1195, 2014, doi:10.4271/2014-01-1195.
10. Turkish, M.C., "3-Valve Stratified Charge Engines: Evolvement, Analysis and Progression," SAE Technical Paper 741163, 1974, doi:10.4271/741163.
11. Noguchi, N., Sanda, S. and Nakamura, N., "Development of Toyota Lean Burn Engine," SAE Technical Paper 760757, 1976, doi:10.4271/760757.
12. Gussak, L.A., Karpov, V.P. and Tikhonov, Y.Y., "The Application of the Lag-Process in Pre-chamber Engines," SAE Technical Paper 790692, 1979, doi:10.4271/790692.
13. Maxson, J.A., Hensinger, D.M., Horn, K., and Oppenheim, A.K., "Performance of Multiple Stream Pulsed Jet Combustion Systems," SAE Technical Paper 910565, 1991, doi:10.4271/910565.
14. Latsch, R., "The Swirl Chamber Spark Plug: A Means of Faster, More Uniform Energy Conversion in the Spark Ignition Engine," SAE Technical Paper 840455, 1984, doi: 10.4271/840455.
15. Toulson, E., Watson, H.C., and Attard, W.P., "Gas Assisted Jet Ignition of Ultra-Lean LPG in a Spark Ignition Engine," SAE Technical Paper 2009-01-0506, 2009, doi: 10.4271/2009-01-0506.
16. Lezanski, T., Kesler, M., Rychter, T., Teodorczyk, A., and Wolanski, P., "Performance of a Pulsed Jet Combustion (PJC) System in a Research Engine," SAE Technical Paper 932709, 1993, doi:10.4271/932709.

17. Kito, S., Wakai, K., Takahashi, S., Fukaya, N., and Takada, Y., Ignition Limit of Lean Mixture by Hydrogen Flame Jet Ignition. JSAE Review, 2000. 21(3): 373-378.
18. Couet, S., Higelin, P., and Moreau, B., "APIR: A New Firing Concept for the Internal Combustion Engines -Sensitivity to Knock and In-Cylinder Aerodynamics," SAE Technical Paper 2001-01-1954, 2001, doi: 10.4271/2001-01-1954.
19. Kettner, M., Rothe, M., Velji, A., Spicher, U., Kuhnert, D., and Latsch, R., "A New Flame Jet Concept to Improve the Inflammation of Lean Burn Mixtures in SI Engines" SAE Technical Paper 2005-01-3688, 2005, doi:10.4271/2005-01-3688.
20. Najt, P.M., Rask, R.B., and Reuss, D.L., Dual Mode Engine Combustion Process. 2003: United States Patent No.6595181.
21. Kojic, A., Hathout, J.-P., Cook, D., and Ahmed, J., Control of Auto-Ignition Timing for Combustion in Piston Engines by Prechamber Compression Ignition. 2005: United States Patent No. PCT/US2004/029612.
22. Pape, J., Getzlaff, J., Gruenig, C., Kuhnert, D., and Latsch, R., "Investigations on Pre-Chamber Spark Plug with Pilot Injection," SAE Technical Paper 2007-01-0479, 2007, doi:10.4271/2007-01-0479.
23. Regueiro, J., "The Case for New Divided-Chamber Diesel Combustion SystemsPart Two: Critical Analysis of, and Solutions for, Swirl-Prechamber Engines," SAE Technical Paper 2001-01-0274, 2001, https://doi.org/10.4271/2001-01-0274.
24. Toulson, E., Watson, H., and Attard, W., "Gas Assisted Jet Ignition of Ultra-Lean LPG in a Spark Ignition Engine," SAE Technical Paper 2009-01-0506, 2009, https://doi.org/10.4271/2009-01-0506.
25. Toulson, E., Schock, H., and Attard, W., "A Review of Pre-Chamber Initiated Jet Ignition Combustion Systems," SAE Technical Paper 2010-01-2263, 2010, https://doi.org/10.4271/2010-01-2263.
26. Galloni E, Fontana G, Palmaccio R. Effects of exhaust gas recycle in a downsized gasoline engine. Appl Energy 2013;105: 99-107.
27. Stein, Robert A., et al. "Effect of heat of vaporization, chemical octane, and sensitivity on knock limit for ethanol-gasoline blends." SAE International Journal of Fuels and Lubricants 5.2012-01-1277 (2012): 823-843.
28. Moxey, Ben G., Alasdair Cairns, and Hua Zhao. A Study of Turbulent Flame Development with Ethanol Fuels in an Optical Spark Ignition Engine. SAE Paper 2014-01-2622, 2014.

414